Climate-Dependent Performance of Solar-Powered Spray Cooling Canopies: A Climate-Archetype Framework for Pre-Deployment Feasibility Assessment

Coskun Firat * and Asfaw Beyene

Posted Date: 11 May 2026

doi: 10.20944/preprints202605.0695.v1

Keywords: urban heat island; evaporative cooling; photovoltaic energy autonomy; adaptive misting control; climate archetype; pre-deployment screening

 doi:10.20944/preprints202605.0695.v1

Article

Climate-Dependent Performance of Solar-Powered Spray Cooling Canopies: A Climate-Archetype Framework for Pre-Deployment Feasibility Assessment

Coskun Firat [1,*] and Asfaw Beyene [2]

[1] Energy Institute, Istanbul Technical University, Istanbul, Türkiye

[2] Department of Mechanical Engineering, San Diego State University, San Diego, CA, USA

* Correspondence: coskun.firat@itu.edu.tr

Abstract

This research examines how climate change intensifies urban heat stress, particularly in public spaces where mechanical cooling is impractical. A climate-driven, systems-level numerical model is developed to evaluate the pre-installation feasibility of portable, solar-powered misting canopies. Hourly Typical Meteorological Year data (TMYx, 2009–2023) are analyzed for each city to estimate photovoltaic (PV) energy yield, electrical load, potential misting duration, water demand, and PV-to-load autonomy under summer daytime conditions. Misting operation is governed by an adaptive, rule-based control strategy based on air temperature, relative humidity, and solar radiation. To enable systematic comparison, K-means clustering is applied to classify the cities into six archetypal summer climate zones. Results indicate that evaporative cooling feasibility is driven more by ambient humidity than by air temperature. Hot-dry interior cities achieve the longest average misting duration (502.65 hours) and highest water consumption (30,486 L per module), but exhibit the lowest PV-to-load autonomy ratio (1.53) due to high energy demand for pumping. In contrast, humid Black Sea cities show minimal misting duration (13.11 hours) and water use (478 L) yet achieve the highest autonomy (40.91) because of limited system operation. It is important to note that the autonomy ratio reflects a seasonal energy balance rather than continuous off-grid capability. Overall, the adaptive control approach effectively aligns water and energy use with climatic suitability across all clusters. The proposed framework offers a scalable and quantitative screening tool to inform the design and deployment of PV-powered outdoor cooling systems across diverse urban environments.

Keywords: urban heat island; evaporative cooling; photovoltaic energy autonomy; adaptive misting control; climate archetype; pre-deployment screening

1. Introduction

The broader dynamics of urban heat stress and mitigation can be examined within a unified analytical framework. The expansion of cities, coupled with climate change, has intensified heat stress globally. Although cities occupy only about 2% of the Earth's land surface, they concentrate more than half of the global population and over 75% of total energy consumption. As demonstrated by Johri et al. [1], this density generates a positive feedback loop in which anthropogenic heat and waste energy emissions continuously elevate urban temperatures. Jabbar et al. [2] further characterize this as the Urban Heat Island (UHI) effect—not merely a condition of overheating, but a systemic outcome of urban form, including high density, impermeable surfaces, limited vegetation, and restricted airflow, which together trap radiative, convective, and sensible heat.

Across the 110 cities analyzed as case studies, these mechanisms manifest with varying intensity depending on climatic and urban characteristics. The energy implications of UHIs are well

 doi:10.20944/preprints202605.0695.v1

documented and exhibit a pronounced seasonal asymmetry. De Souza [3] quantified that urban heating demand may decrease by approximately 22% relative to rural areas, while cooling demand increases by about 25% under UHI conditions. Santamouris et al. [4] showed that in Athens, UHI intensities exceeding 10 °C during heatwaves led to a doubling of cooling demand, a threefold increase in peak electricity load, and a 25% reduction in air-conditioning efficiency. Similarly, Zhang et al. [5] projected a fivefold increase in cooling-related CO_2 emissions in London by 2050, while Takane et al. [6] estimated that electricity demand in central Tokyo increases by 6.6% per 1 °C rise in ambient temperature. Interpreted through the 110-city dataset, these findings confirm that summer cooling demand is becoming the dominant urban energy stressor, with direct consequences for grid stability, emissions, and resilience.

In addition to building energy demand, elevated urban temperatures degrade outdoor environmental quality. As noted by Jabbar et al. [2], UHI effects contribute to reduced thermal comfort, limited nighttime cooling, increased air pollution, and higher rates of heat-related illness and mortality. These impacts are not evenly distributed. Schlosberg [7] emphasizes that climate-related risks in cities disproportionately affect vulnerable populations with limited adaptive capacity. Across the 110 cities, this inequity is particularly relevant in public open spaces—such as plazas, pedestrian corridors, bus stops, and playgrounds—which are essential for mobility and social interaction yet highly exposed to heat stress. Consequently, mitigating outdoor heat exposure remains a central objective of climate-responsive urban design.

A range of UHI mitigation strategies has been explored, though each presents limitations when assessed across diverse climatic conditions. Jandaghian and Colombo [8] found that urban water bodies can provide localized cooling through evapotranspiration and thermal mass, but their effectiveness depends strongly on size, surrounding geometry, and wind conditions. Reflective materials, including cool roofs and pavements, can reduce surface temperatures by 6–10 °C [9], yet their large-scale implementation is often constrained by cost, space, and disruption. Green infrastructure strategies—such as trees, parks, and green roofs—have been shown to reduce air temperatures by 2–8 °C through shading and evapotranspiration [10], although their performance depends on irrigation, substrate conditions, and building typology [11]. Irfeey et al. [12] further note that such strategies may respond too slowly under extreme and acute heat conditions. When considered across the 110 cities, these approaches are generally permanent, capital-intensive, and difficult to deploy rapidly in dense or resource-constrained environments.

Water-based evaporative cooling offers a more flexible alternative. Almusaed [13] describes the thermodynamic basis of misting, where fine water droplets absorb latent heat from the surrounding air during evaporation, thereby reducing dry-bulb temperature without mechanical cooling. Field studies have demonstrated its effectiveness in outdoor environments. Ulpiani et al. [14] reported air temperature reductions of 3–5 °C under Mediterranean summer conditions, with 67–91% of occupants experiencing improved thermal comfort, particularly under high solar radiation and light wind (1–2 m/s). Tian and Li [15] observed a maximum cooling effect of 5.68 °C under hot-humid conditions, while Gao et al. [16] recorded a 3.1 °C reduction at bus stops in subtropical Guangzhou, achieving over 80% thermal acceptability within ten minutes. Despite these promising results, such studies are typically limited to single locations, restricting their applicability across broader climatic ranges. The inclusion of 110 cities in this study addresses this limitation by enabling systematic evaluation of climatic transferability and operational thresholds.

Advances in adaptive and sensor-based control aim to improve the efficiency of misting systems. Stojanovic et al. [17] developed a context-aware system incorporating occupancy sensing and predictive algorithms, demonstrating reduced water consumption without compromising comfort. Ulpiani and Zinzi [18] implemented smart controls in a hybrid outdoor cooling shelter, though their approach remained site-specific. Threshold-based control strategies explored by Eduard et al. [19] and Malbog et al. [20] offer relevant logic-based frameworks but lack integration with long-term climate variability, PV generation, and water resource constraints. The 110-city analysis extends these approaches by linking adaptive control to both climatic conditions and renewable energy availability.

 doi:10.20944/preprints202605.0695.v1

Parallel research on photovoltaic (PV) integration in urban environments highlights the potential for decentralized energy generation. Formolli et al. [21] showed that distributed PV systems can effectively offset local electricity demand, though regulatory and technical barriers persist. Santos et al. [22] demonstrated that even small-scale PV installations on bus shelters can generate significant electricity, but did not consider coupling with cooling demand. Similarly, Alikhanova et al. [23] and Sanchez-Aparicio et al. [24] focused on PV performance under specific climatic conditions without addressing thermal comfort or water-energy interactions. Abdulmouti et al. [25] discussed PV integration conceptually at the urban scale, while Ouyang et al. [26] showed that artificial shading structures can provide thermal benefits comparable to trees under extreme conditions. Across these studies, PV systems are generally treated as standalone energy solutions.

By contrast, the 110-city framework adopted here enables a coupled assessment of PV generation and evaporative cooling demand. This integrated perspective reveals the potential for synergistic system design, where solar energy directly supports adaptive misting operation in outdoor public spaces. Rather than isolated case studies, the 110 cities collectively represent a wide spectrum of climatic and urban conditions, allowing for a scalable and comparative evaluation of PV-powered cooling strategies across diverse environments.

Using the same 110 cities across Türkiye as case studies, the present work positions existing research within a broader, climate-comparative perspective. Both urban evaporative cooling and solar-integrated street furniture have received increasing attention; however, a critical gap remains in their combined assessment across diverse climatic contexts. To date, no robust and climate-transferable framework has been developed that simultaneously evaluates photovoltaic (PV) energy independence, adaptive misting performance, and water demand for modular outdoor cooling systems at a regional or national scale.

Across the 110-city dataset, this gap becomes particularly evident. Existing studies are largely constrained to single-site experimental demonstrations under specific climatic conditions [14,18], limiting their generalizability. Others focus on indoor or agricultural misting applications [19,20], which are not directly applicable to uncontrolled outdoor urban environments. In parallel, PV-focused studies [22,24] typically assess energy generation in isolation, without addressing cooling performance or the coupling between water and energy systems. As a result, there is no comprehensive understanding of how ambient humidity, air temperature, and solar irradiance jointly influence the operational feasibility of solar-powered evaporative cooling across different climates.

Furthermore, while climatic classification approaches are widely used in building science, their application to outdoor thermal adaptation technologies remains underexplored. In particular, no prior study has employed climate archetype classification to derive transferable, pre-deployment feasibility benchmarks for PV-powered misting systems in public spaces. The 110 cities considered here provide a sufficiently diverse climatic sample to enable such classification and comparative analysis.

This study addresses these gaps through a design-driven, system-level numerical framework that integrates PV energy modeling, rule-based adaptive misting control, and climate-dependent water consumption across 110 locations using hourly TMYx data (2009–2023). The novelty of the work is threefold. First, it represents one of the first efforts to evaluate the climate-dependent, joint performance of PV energy autonomy and evaporative cooling at a national scale using a consistent and reproducible methodology. Second, it introduces k-means-based summer climate archetype classification—based on temperature, humidity, solar irradiance, and wind speed—as a transferable tool for feasibility screening. Third, it defines explicit quantitative climatic thresholds under which modular solar-powered spray cooling canopies can achieve high energy autonomy with controlled water use, offering actionable insights for urban design, energy engineering, and climate adaptation policy.

Accordingly, this study aims to:

 doi:10.20944/preprints202605.0695.v1

1. Establish a system-level numerical framework coupling photovoltaic generation, battery storage, and adaptive spray cooling control under real outdoor weather conditions.
2. Evaluate energy self-sufficiency, achievable misting duration, and water consumption across 110 cities using hourly TMYx climate data (2009–2023).
3. Classify these cities into summer climate archetypes using k-means clustering and define performance benchmarks associated with each archetype, enabling transferable design and deployment strategies for modular solar-powered cooling canopies in public spaces.

2. Methodology

Building on the 110-city case study framework, this study develops a climate-informed, system-level numerical methodology to evaluate the pre-deployment feasibility of modular solar-powered spray cooling canopies (MSPSCCs) under realistic outdoor conditions. The approach integrates photovoltaic (PV) energy generation, rule-based adaptive misting control, and water consumption modeling, applied consistently across all locations using long-term hourly TMYx climate data.

Rather than resolving detailed microscale phenomena such as pedestrian-level airflow or droplet dispersion, the methodology is intentionally structured as a pre-deployment screening tool. Its primary objective is to identify the climatic conditions under which the system can operate effectively, defined in terms of high PV-to-load autonomy and controlled water demand, across a wide range of urban environments represented by the 110 cities.

Figure 1 presents a block diagram of the simulation framework, outlining inputs, processing stages, and output indicators. The primary inputs consist of seven TMYx weather variables—dry-bulb temperature, relative humidity, global horizontal irradiance (GHI), direct normal irradiance (DNI), diffuse horizontal irradiance (DHI), wind speed, and precipitation—along with static system parameters detailed in Appendix A. These inputs feed into four interconnected modules: (i) solar geometry and irradiance transposition, (ii) PV power generation and battery storage modeling, (iii) adaptive misting control logic, and (iv) water consumption estimation.

The simulation produces five key performance indicators (defined in Section 2.4.5), which are evaluated for each of the 110 cities on an hourly basis. Aggregated climatic and performance metrics are then used as inputs for k-means clustering, Figure 1, enabling the classification of cities into distinct summer climate archetypes. This structure allows both location-specific analysis and generalized, climate-based comparison, ensuring that the findings are transferable beyond individual case studies.

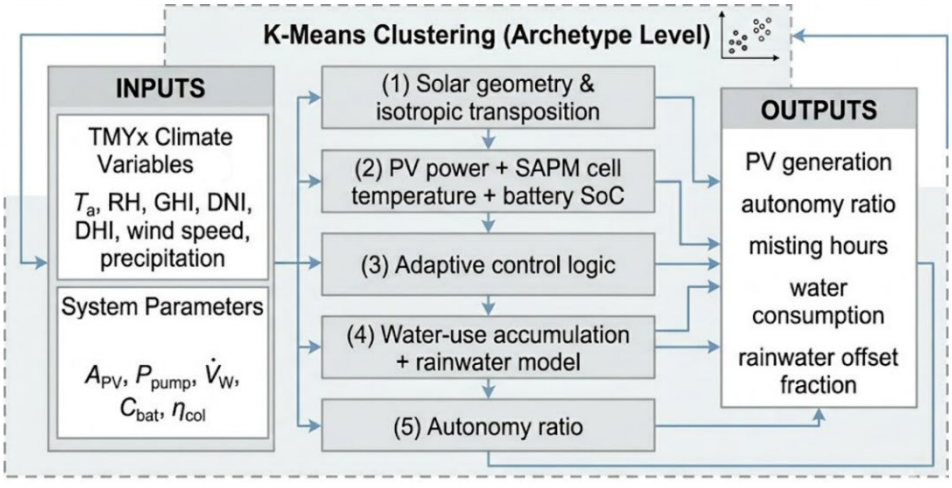

Figure 1. Simulation framework for evaluating the MSPSCC system, integrating TMYx climate inputs, PV energy modeling, adaptive misting control, and water-use estimation, with k-means clustering used to derive climate archetypes.

2.1. System Design Framework

 doi:10.20944/preprints202605.0695.v1

The MSPSCC is imagined as a quick-deployment urban cooling application that is structured around four principles that drive its physical and operational design: adaptive design (interactive misting control), modular design (scalable kit-of-parts deployment), energy and resource autonomy (on-site photovoltaic generation and rainwater augmentation) and urban integration (lightweight and context-sensitive structure). These principles are elaborated in Section 3 and quantified for the numerical model in Appendix A.

2.2. System Design Specifications

2.2.1. Module Geometry

The nominal size of each section of the canopy structure is approximately 4m x 4m. The overhead shading surface above the module consists of PV panel; the underside surface of the module contains the mist distribution manifold. In this work, based on the numerical simulations conducted, the active PV area for one module is normalized to 1m² and the given energy and autonomy values scale linearly with PV area for any installation.

2.2.2. Photovoltaic System

Crystalline silicon PV panels are expected to have a temperature coefficient of γ=−0.004 °C^{-1} [28] and an STC efficiency of η_{pv}=0.20. Modules are set, face south, and have an inclination according to the local latitude. Energy flow between PV generation, battery storage, and loads is controlled by a charge controller. A usable capacity of 1.0 kWh per module, a round-trip efficiency of 0.90, and SoC constraints of 10-90% define battery storage.

Rather than a suggested design limit, the 1 m² PV area serves as a normalisation foundation. Depending on structural, daylighting, and aesthetic limitations, a 4 m × 4 m canopy might physically hold 8-12 m² of PV covering. As a result, autonomy ratios can be scaled linearly for any other PV coverage; For instance, assuming constant load and module alignment, 2-3 m² of active PV area per module would almost double or triple the given range of autonomy values.

2.2.3. Misting Subsystem

Tiny-mist nozzles generate droplets between tens of microns to microns in size, therefore encouraging full evaporation and reducing surface wetting [14,18]. It is assumed that each module has a full duty cycle baseline water flow rate of 2.0 L min^{-1}. A filter unit lowers the possibility of nozzle clogging.

2.2.4. Electrical Loads

System electrical demand includes the misting pump (250 W when it is running), the control unit and sensors (8 W when they are on), and standby electronics (2 W when the misting is off). The pump controls total active demand, which is 258 W. Appendix A (Table A1) lists all baseline values.

2.3. Numerical Performance Model

2.3.1. Photovoltaic Energy Model

Hourly PV power output is estimated using a PVWatts-type formulation [28]:

$$P_{PV}(t) = \eta_{PV} A_{PV} G_{POA}(t) \left[1 + \gamma\left[T_c(t) - T_{ref}\right]\right] \quad (1)$$

where $G_{POA}(t)$ is plane-of-array irradiance derived from EPW components (GHI, DNI, DHI) using standard solar geometry and an isotropic sky transposition model. Cell temperature $T_c(t)$ is estimated using the SAPM empirical expression with glass/polymer open-rack coefficients (a = −3.56, b = −0.075) [28]:

$$T_c(t) = T_a(t) + G_{POA}(t) \exp\left(a + b \cdot v_{wind}(t)\right) \quad (2)$$

 doi:10.20944/preprints202605.0695.v1

2.3.2. Adaptive Misting Control Logic

At each hourly time step, misting is activated only when all three environmental conditions are simultaneously satisfied:

(1) Air temperature: $T_a(t) \geq T_{set} = 32$ °C, which is in line with the universal thermal climate index (UTCI) moderate heat-stress threshold for people who are not active outside [27] and agrees with field studies that used misting in real life [14,18].

(2) Above $RH(t) \leq RH_{max} = 65\%$, relative humidity: fine-mist evaporation is significantly reduced and surface wetting risk is enhanced [16].

(3) Plane-of-array irradiance: $G_{poa}(t) \geq G_{min} = 200$ W m^{-2} limits activation to times of significant PV production and high solar radiative load on residents.

The duty-cycle factor $f_{on}(t)$ controls partial-load functioning when all activation criteria are met. The temperature component rises linearly from 0.25 to 1.0 as T_a rises from T_{set} to $T_{set} + \Delta T$ (where $\Delta T = 8$ °C), reflecting higher cooling benefit under increasing heat stress. The humidity element drops as RH nears RH_{max}, which shows less evaporative potential and more wetting risk at high humidity. Therefore, the highest duty cycles happen when it's hot and not too wet, but when the humidity gets close to the deactivation threshold, duty goes down. At all dormant time steps, 2 W of standby power is applied.

2.3.3. Energy Autonomy Metric

The PV-to-load autonomy ratio is:

$$\alpha = \sum_t E_{pv}(t) \Big/ \sum_t E_{load}(t) \tag{3}$$

with $E_{pv}(t)$ being hourly PV energy generation (Wh) and $E_{load}(t)$ being the hourly PV load of pump, controller, sensors, and standby electronics (Wh). The autonomy ratio α is a seasonal energy-balance ratio and does not ensure that hourly PV output matches hourly load. Hourly imbalances can occur and are dependent on battery storage, dispatch rules and storage efficiency; α is therefore viewed as a dimensionless screening tool, rather than a complete off-grid reliability metric. Seasonal PV surplus occurs for $\alpha > 1.0$; the ratio is directly proportional to PV area.

2.3.4. Water Consumption and Rainwater Harvesting

Hourly water consumption is computed as:

$$W_{use} = \sum_t [\dot{m}_w \cdot n_{noz} \cdot \Delta t \cdot f_{on}(t)] \tag{4}$$

where $\dot{m}_w$ is nozzle flow rate (L min^{-1}), $\cdot n_{noz}$ is the number of active nozzles, $\Delta t = 60$ min, and $f_{on}(t)$ is the duty-cycle fraction. Rainwater harvesting potential is estimated as:

$$W_{harv} = A_{catch} R \eta_{col} \tag{5}$$

where A_{catch} is the module catchment area (m²), R is summer precipitation depth (m), and $\eta_{col} = 0.80$ is the collection efficiency. This model does not resolve precipitation timing relative to misting demand; a storage-routing model is needed for site-specific design.

2.4. Climate Data and Archetype Classification

2.4.1. Climate Dataset

Using the 110 cities across Türkiye as case studies, system performance is evaluated through a consistent and high-resolution climatic dataset. Hourly Typical Meteorological Year data (TMYx, 2009–2023) were obtained from the OneBuilding repository [29] for all locations. The dataset includes dry-bulb air temperature, relative humidity, global horizontal irradiance (GHI), direct normal irradiance (DNI), diffuse horizontal irradiance (DHI), wind speed, and precipitation.

The selection of these 110 cities ensures representation of the full climatic diversity of Türkiye, including hot-dry inland basins, semi-arid plateau regions, humid Black Sea and Mediterranean

 doi:10.20944/preprints202605.0695.v1

coastal zones, and cold continental highlands. Within this dataset, performance calculations are restricted to the summer period (June–August) and daytime operating hours (10:00–18:00 local solar time), corresponding to peak outdoor heat stress and maximum solar availability. This temporal filtering ensures that the analysis directly targets the conditions under which outdoor cooling interventions are most critical across all case-study locations.

2.4.2. K-Means Climate Archetype Classification

To enable systematic comparison across the 110 cities, locations are grouped into six summer climate archetypes using k-means clustering. The clustering is based on five standardized variables derived from summer daytime conditions: mean air temperature (T_a), 95th-percentile T_a, mean relative humidity (RH), mean GHI, and mean wind speed. Rather than using raw hourly time series, clustering is performed on aggregated site-level statistics, ensuring that each city is represented by its characteristic summer climate profile.

All variables are standardized to zero mean and unit variance prior to clustering. The number of clusters ($k = 6$) is selected using the within-cluster sum-of-squares elbow criterion, which shows a clear inflection point at $k = 6$, beyond which reductions in inertia become marginal. Although the silhouette coefficient does not exhibit a distinct maximum—an expected outcome for geographically continuous and partially overlapping climate regimes—the selected clustering yields interpretable and physically meaningful archetypes. Within the 110-city framework, this classification enables the identification of recurring climatic patterns and supports the derivation of transferable performance benchmarks for PV-powered misting systems.

2.5. Model Assumptions, Scope, and Limitations

The methodology, applied uniformly across the 110 cities, is designed as a pre-deployment screening tool rather than a detailed microclimate simulation. It does not resolve droplet trajectories, airflow fields, or pedestrian-level thermal comfort metrics; instead, it evaluates operational feasibility in terms of energy balance, achievable misting duration, and water demand.

To ensure comparability across all case-study locations, system parameters are held constant, and site-specific optimization is not performed at this stage. Consequently, the results should be interpreted as relative performance indicators between cities rather than precise predictions for individual sites.

Simplifications are also present in subsystem modeling. The battery model neglects inverter losses and long-term degradation effects, while the rainwater harvesting component does not resolve sub-daily temporal dynamics. Despite these limitations, the framework provides a consistent basis for comparing how different climatic conditions—represented by the 110 cities—affect system feasibility and resource requirements.

3. System Definition and Deployment Assumptions

Within the context of the 110-city case studies, this section defines the physical and operational characteristics of the modular solar-powered spray cooling canopy (MSPSCC) used as the reference system. The objective is not to present a finalized product design, but rather to establish a physically consistent baseline configuration whose performance can be evaluated under diverse climatic conditions. The system characteristics defined here correspond directly to the modeling framework described in Section 2, while principles of operation and adaptive control are detailed in Section 2.1.

3.1. Module Geometry and Deployment Configurations

The fundamental unit of the system is a canopy module with nominal dimensions of 4 m × 4 m. Each module consists of vertical supports, an overhead canopy integrating photovoltaic panels on the upper surface, and a misting manifold on the underside, along with integrated power and water distribution lines.

 doi:10.20944/preprints202605.0695.v1

Across the 110 cities, this modular unit is assumed to be deployable in three primary configurations: (i) a standalone module for localized applications such as bus stops or seating areas; (ii) a linear array forming a continuous shaded corridor, which constitutes the primary configuration analyzed in this study; and (iii) a tessellated cluster arrangement for larger public spaces such as plazas.

Because the analysis is conducted at the module level, the performance results derived from the 110 case-study cities are directly scalable to all deployment configurations. The linear configuration, representative of pedestrian pathways and transit corridors, is illustrated in Figure 2 and serves as the reference scenario for evaluating system performance across diverse urban climates.

Top of Form

Bottom of Form

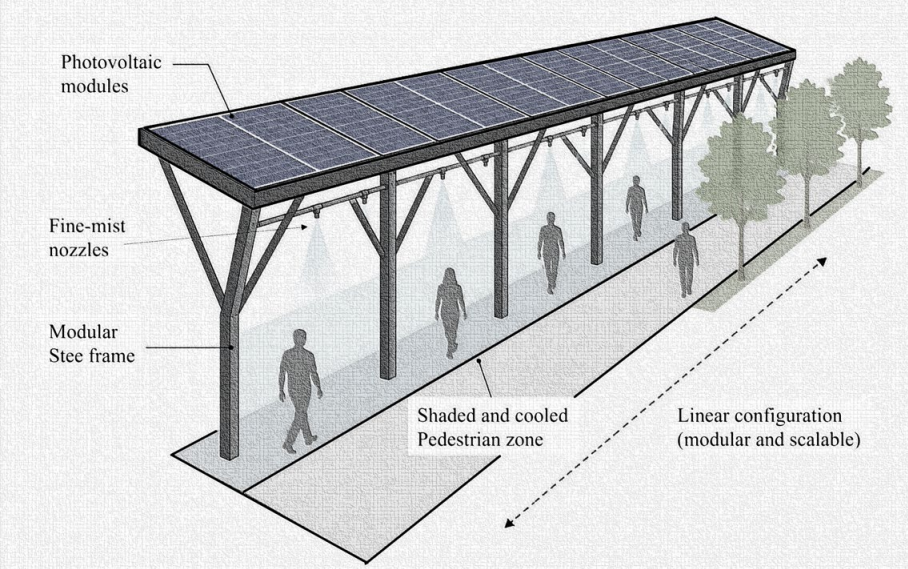

Figure 2. Schematic representation of the MSPSCC system in linear deployment configuration, showing PV canopy modules, shading footprint, and distributed misting zones.

3.2. PV Integration and Misting Layout

The top canopy surface is a dual-purpose PV surface providing on-site electricity generation and direct shading of the pedestrian zone. The same structural element that prevents shortwave radiation from penetrating to the occupants is the source of electricity that drives the misting pump, the main functional synergy of the MSPSCC. The misting manifold is placed on the inner canopy edge below the PV surface providing fine-mist discharge over the pedestrian area. Main structural elements are lightweight recycled aluminum or steel beams; facades and shading elements are detachable for aesthetic personalization. Temporary or seasonal use is possible owing to non-permanent foundations (weighted bases or shallow anchors).

3.3. Connection Between System Definition and Performance Evaluation

Table 1 presents each physical system parameter to the model equation in which it appears, establishing full traceability between the system concept and the numerical results of Section 4.

Table 1. Mapping of physical system parameters to numerical model equations.

Physical system parameter	Value / assumption	Model equation
Module plan footprint	4 m × 4 m	Eq. (5)—canopy catchment area
Active PV area (normalized)	1 m² per module	Eq. (1)—PV power output
PV efficiency (STC)	$\eta_{pv} = 0.20$	Eq. (1)—PV power output
Temperature coefficient of power	$\gamma = -0.004\ °C^{-1}$	Eq. (1)—PV power output

 doi:10.20944/preprints202605.0695.v1

Pump electrical demand (active)	250 W	Eq. (3)—energy autonomy ratio
Nozzle flow rate (full duty)	2.0 L min^{-1} per module	Eq. (4)—water consumption

4. Results and Discussion

In this section, the climate performance assessment of the MSPSCC is presented for the cities selected for the case study using hourly TMYx (2009-2023) data, and insights are provided for deployment, resource planning and urban cooling strategies. All values are for the summer daytime period (June-August, 10:00-18:00) and per 1 m^2 of PV area, unless otherwise noted.

4.1. Summer Climate Characteristics and Misting Feasibility

Figure 3 shows the mean summer daytime air temperature and relative humidity of the case study cities, colored by archetypes. While average temperatures are between about 25 °C and over 33 °C in summer, average relative humidity lies between about 24% for interior basins to 62% for coastal regions on the Black Sea.

A main conclusion is that relative humidity, not air temperature, is the main factor controlling the feasibility of misting. Sites with similar summer temperatures might have a mean RH that differs by more than 40 percentage points, which would cause totally different misting activation patterns. Interior areas that are hot and dry have the highest temperatures and lowest humidity. This makes conditions where the RH deactivation threshold of 65% is hardly ever binding and misting runs for long time. Locations on the humid Black Sea have consistently high humidity, sometimes higher than RH_{max}, which significantly limits activation.

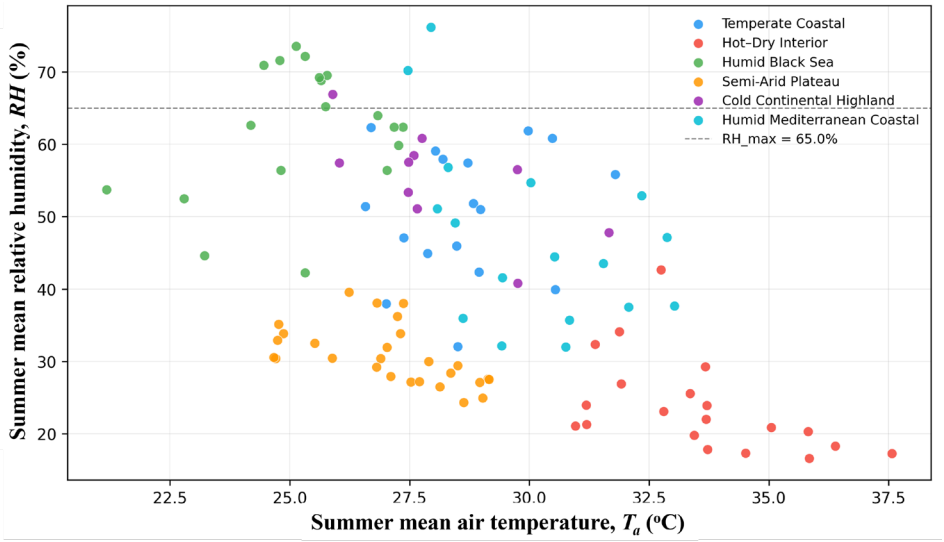

Figure 3. Mean summer daytime air temperature (T_a) and relative humidity (RH) across the selected EPW locations, grouped into six climate archetypes. The dashed horizontal line indicates RH_{max} = 65%. Relative humidity rather than temperature alone determines evaporative cooling feasibility.

Table 2 summarizes mean summer climate characteristics and system performance metrics for each archetype. Hot-Dry Interior locations record the longest mean misting duration (502.65 h) and highest mean water consumption (30 486 L per module), driven by near-continuous satisfaction of all three control conditions. Humid Black Sea locations record only 13.11 h of misting and 478 L per module, a 38-fold difference in misting hours and 64-fold difference in water use relative to the Hot-Dry Interior archetype.

Table 2. Mean summer daytime climate characteristics and system performance metrics for the six identified climate archetypes (TMYx 2009-2023). Analysis period: June-August, 10:00-18:00. PV generation and autonomy

 doi:10.20944/preprints202605.0695.v1

ratio are normalized per 1 m² of installed PV area. Autonomy ratios above 1.0 indicate that cumulative PV generation exceeds cumulative system electrical demand over the evaluation period.

Climate archetype	N	Mean T_a (°C)	Mean RH (%)	Mean GHI (Wm^{-2})	Autonomy ratio (–)	Water use (L/module)	Misting hours (h)
Cold Continental Highland	10	28.1	55.1	661.2	24.57	3 466	97.00
Hot–Dry Interior	20	33.5	23.7	722.2	1.53	30 486	502.65
Humid Black Sea	19	25.2	62.0	596.7	40.91	478	13.11
Humid Mediterranean Coastal	17	30.1	47.0	711.2	12.08	9 573	234.18
Semi-Arid Plateau	27	27.1	30.8	682.5	13.03	4 312	99.33
Temperate Coastal	17	28.6	50.6	626.8	7.41	5 709	145.12

4.2. Solar Energy Yield and PV-To-Load Autonomy

Fig. 4 plots summer PV energy generation per unit PV area against the seasonal electrical load, across all the case study locations. PV generation varies within a narrow band of approximately 70-95 kWh m^{-2}, reflecting Türkiye's broadly favorable solar resource. Electrical load varies by more than two orders of magnitude, driven almost entirely by differences in feasible misting duration and duty cycle. In humid locations, the seasonal load is dominated by the 2 W standby draw and is very small. In Hot-Dry Interior locations, 258 W of active demand accumulated over 502.65 hours generates a large seasonal load that a 1 m² PV panel can only marginally offset.

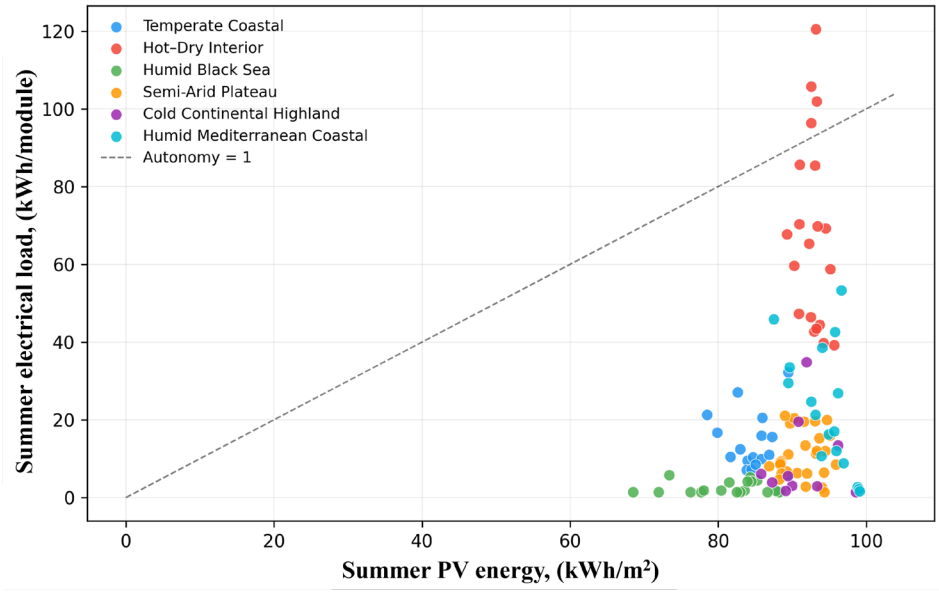

Figure 4. Summer PV energy per unit area (kWh m^{-2}) versus seasonal electrical demand across the referenced locations, colored by climate archetype. The dashed line (α = 1) indicates equality between PV generation and load.

The horizontal box plot in Figure 5 shows the PV-to-load autonomy ratio by archetype. Cooling effectiveness is inversely correlated with the autonomy ratio: The Hot-Dry Interior design has a lower mean autonomy ratio (1.53) as its high misting demand roughly balances its seasonal PV yield from a 1 m² panel; the design type where evaporative cooling is most viable. Near-zero misting activation leaves practically all PV generation as surplus, therefore the Humid Black Sea archetype has the highest autonomy ratio (40.91). This outcome emphasizes a very important interpretive point: In hot regions, great independence denotes little system activation rather than great cooling utility. With a PV-area of 2-3 m² per module, the autonomy ratio of Hot-Dry Interior would increase to roughly 3.0-4.6, providing more comfortable energy surplus for intense misting.

 doi:10.20944/preprints202605.0695.v1

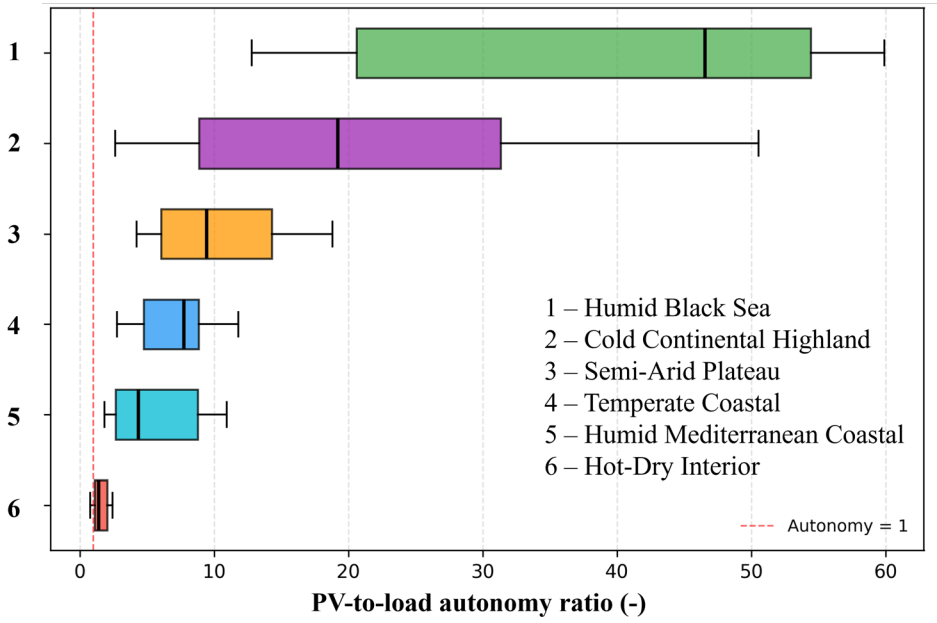

Figure 5. PV-to-load energy autonomy ratio by climate archetype. Horizontal box plots show median (line) and interquartile range; the dashed line ($\alpha = 1$) marks PV-load equality. Archetypes are ordered by median autonomy.

4.3. Water Consumption and Adaptive Control Behavior

For each of the 110 case study locations, Figure 6 plots potential misting length versus overall summer water consumption. Equation (4), which is based on the duty cycle, shows a close-to-linear link for every archetype. The link's slope varies depending on the archetype, from around 36 L/h in the Humid Black Sea to 61 L/h in the Hot-Dry Interior, therefore demonstrating how variations in mean duty cycle brought on by surrounding temperature and humidity influence it. Warmer and drier areas use more water every hour because they turn on the misting system more often (around 1.0). Colder or more humid places use less water because they turn on the misting system less often.

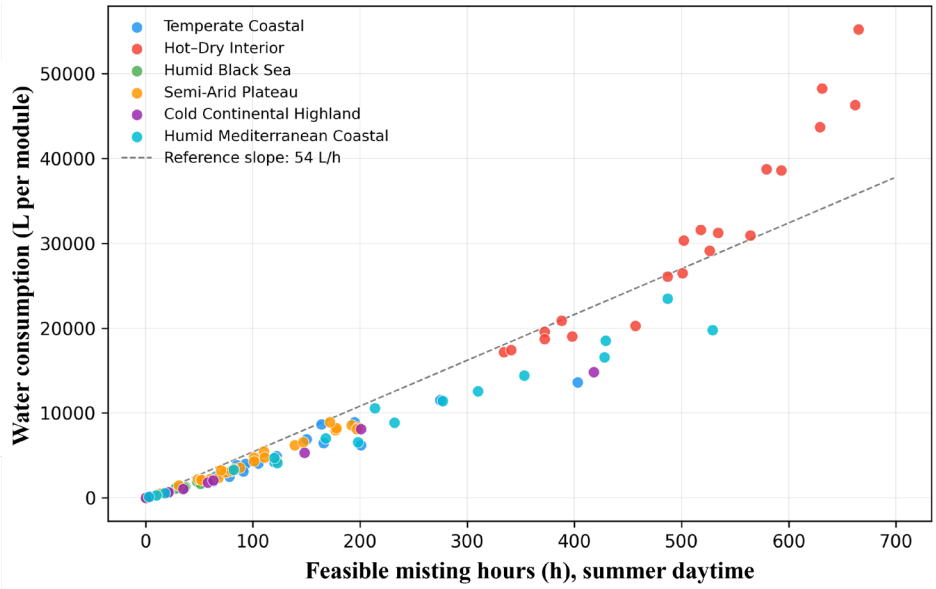

Figure 6. Feasible misting duration versus summer water consumption per module across the EPW locations, grouped by climate archetype. The near-linear trend within each archetype reflects duty-cycle-based water-demand scaling.

Mean summer water demand decreases from 478 L per module in the Humid Black Sea pattern to 30,486 L in the Hot-Dry Interior patterns. The adaptive control naturally restricts water use to times

 doi:10.20944/preprints202605.0695.v1

of climatic appropriateness, thereby lowering the likelihood of ineffective functioning in inappropriate situations. However, a crucial deployment barrier in Hot-Dry Interior areas, where summer precipitation is also lowest, is the high-water demand, necessitating municipal supply connection, cistern storage, or integration with non-potable water sources such greywater recycling or reclaimed irrigation supply.

4.4. Climate-Archetype Profiles and Deployment Implications

The six archetypes define distinct operational regimes with specific implications for system sizing, resource planning, and deployment strategy.

Hot-Dry Interior. This archetype with highest thermodynamic potential in evaporative cooling is the archetype with the largest resource requirements: misting at 502.65 h, water at 30 486 L per module and autonomy at only 1.53 at 1 m^2 PV normalization. At this point, an increase of PV area to 2-3 m^2 per module should be considered, and a connection to the municipal water supply or a cistern would be unavoidable. This archetype would be the main high-benefit target for deployment of MSPSCC.

Semi-Arid Plateau. Moderate temperatures and intermediate humidity produce a balanced profile: 99.33 h misting, 4 312 L, autonomy 13.03. The baseline 1 m^2 PV configuration provides comfortable surplus. This archetype covers 27 of the 110 locations and represents the widest base for transferable guidance.

Humid Mediterranean Coastal. High temperatures combined with moderate humidity (47.0%) produce meaningful misting activity: 234.18 h, 9 573 L, autonomy 12.08. The system provides passive shading and intermittent active cooling suited to densely visited coastal public spaces. Water demand requires planning relative to municipal infrastructure.

Temperate Coastal. Mean misting of 145.12 h, water demand of 5 710 L, and autonomy of 7.41 are served adequately by the baseline configuration. Wider inter-site variability within this group suggests site-level verification before deployment.

Cold Continental Highland. Though it has high irradiance (661.2 W m^{-2}) and a good autonomy ratio (24.57), misting only runs 97.00 h on average because of moderate temperatures and humidity. The large PV surplus may enable more electrical services than just misting.

Humid Black Sea. Persistently high humidity (62.0%) limits misting to 13.11 h per summer and 478 L of water use. The high autonomy ratio (40.91) reflects near-zero load, not high cooling potential. The system functions almost exclusively as a passive solar shading structure. Alternative comfort strategies not dependent on low ambient humidity are more appropriate as primary interventions in this climate.

Overall, these profiles position the MSPSCC as a complementary, rapidly deployable intervention that fills the response gap left by permanent UHI mitigation strategies, reflective surfaces, green roofs, and urban trees, which are capital-intensive, spatially constrained, and poorly responsive to acute heat events [8–11]. In hot-dry and semi-arid contexts the MSPSCC delivers targeted active cooling where permanent strategies cannot respond rapidly; in persistently humid contexts it retains value as a passive solar shading and PV-powered amenity structure. The climate archetype framework enables planners to identify the appropriate intervention mix before deployment, avoiding resource waste from applying evaporative cooling uniformly across climatically unsuitable locations.

4.5. Applicability and Model Boundaries

The results demonstrate climatic viability across a broad range of Türkiye's locations, but four modeling boundaries must be acknowledged. First, the framework does not resolve pedestrian-level thermal comfort; results describe feasibility and resource demand rather than quantified air temperature reduction or UTCI improvement. Field studies reveal 1-5 °C mist-induced cooling [14–16] under perfect circumstances; nevertheless, a site-specific CFD or field measurement is required to exactly define these findings. Second, control thresholds are unchanged across all climates; Section

 doi:10.20944/preprints202605.0695.v1

4.7 presents a sensitivity study assessing their influence. Third, the basic battery model neither considers multi-day storage dynamics nor factors in inverter losses. In hot-dry interior areas with α around 1.53, a thorough hourly dispatch simulation is recommended. Fourth, the rainwater harvesting system does not address the timing of precipitation in view of misting need; The offset fractions should be viewed as theoretical upper limits in the driest archetypes.

Five principal findings emerge from the system-level performance assessment:

- Relative humidity is the dominant constraint on misting feasibility. Locations with mean summer RH above approximately 55-62% record fewer than 65 misting hours per summer regardless of air temperature, establishing humidity as the primary pre-deployment screening variable.
- The PV-to-load autonomy ratio is inversely related to cooling effectiveness. Hot-Dry Interior locations generate the highest misting load and the lowest autonomy (mean 1.53 at 1 m^2 PV normalization). Humid Black Sea locations achieve the highest autonomy (40.91) driven by near-zero misting activation. High autonomy in humid climates does not indicate high cooling usefulness.
- Water consumption varies by archetype from 478 L to 30 486 L per module, scaling with feasible misting hours at archetype-specific rates of 36-61 L/h. Adaptive control naturally constrains water use to periods of climatic effectiveness, enabling pre-deployment resource planning at city scale.
- The central design trade-off is between cooling benefit and resource demand: hot-dry climates offer the greatest evaporative cooling potential but also the highest water and energy requirements, necessitating larger PV area (2-3 m^2 recommended) and reliable water supply infrastructure.
- The six climate archetypes provide a transferable pre-deployment screening framework applicable to other semi-arid and Mediterranean regions, subject to recalibration of control thresholds using local TMYx data and comfort standards.

4.6. Sensitivity of Control Thresholds

Three static control settings are utilized throughout the performance analysis: T_{set}=32 °C, RH_{max}=65% and G_{min}=200 Wm^{-2}. These thresholds were applied equally to all the 110 case study sites so that comparison between climates would be objective. It is important to recognize that if another setting were chosen, the true amount of usable misting time available, the amount of water consumed and electricity usage would vary.

T_{set} governs how often the system activates during warm, non-extreme conditions. Lowering T_{set} increases misting frequency, water consumption, and pump energy demand, especially in temperate coastal, humid Mediterranean, and highland regions where summer daytime temperatures typically hover near the activation threshold. Conversely, raising T_{set} limits operation in these moderate climates, restricting misting primarily to the hottest zones.

The humidity threshold, RH_{max}, dictates the feasibility of evaporative cooling. A stricter humidity limit restricts operation primarily in humid Mediterranean, temperate coastal, and Black Sea locations, where relative humidity frequently meets or exceeds the baseline threshold. Conversely, Hot-Dry Interior locations remain largely unaffected, as their summer daytime relative humidity stays substantially lower. While the absolute duration of misting and water consumption depend on these thresholds, the ranking of climate archetypes stays consistent: hot-dry climates offer the greatest potential for evaporation, whereas humid climates suffer from constrained cooling capacity.

The irradiance threshold G_{min} primarily restricts misting to periods with sufficient solar availability and elevated daytime heat exposure. Adjusting this threshold would affect marginal morning, late-afternoon, or cloudy-hour operation, but it is unlikely to reverse the main humidity-controlled distinction between hot-dry and humid archetypes.

 doi:10.20944/preprints202605.0695.v1

Accordingly, the baseline threshold set should be interpreted as a transparent screening assumption rather than an optimized control policy. A full parametric sensitivity analysis of T_{set}, RH_{max}, G_{min}, duty-cycle functions, and occupancy schedules is beyond the scope of the present study and should be conducted in future work using site-specific comfort targets and water-resource constraints. The present results therefore provide a consistent comparative baseline for climate-archetype screening, while detailed deployment design should recalibrate the thresholds to local thermal comfort standards, occupancy profiles, and water availability.

5. Conclusions

This study developed and applied a climate-informed, system-level numerical framework to evaluate the pre-deployment feasibility of MSPSCCs as outdoor thermal comfort interventions in urban public spaces. Using hourly TMYx (2009-2023) data for the selected 110 locations and k-means classification into six summer climate archetypes, the framework provides transferable, quantitative guidance on where and under what climatic conditions PV-powered evaporative cooling can operate effectively and sustainably.

The principal findings indicate that relative humidity serves as the dominant constraint on misting feasibility, overriding the influence of air temperature. Hot-Dry Interior locations achieve a mean feasible misting duration of 502.65 hours and a mean water demand of 30,486 liters per module. In contrast, Humid Black Sea locations record only 13.11 hours and 478 liters, a 38-fold difference in duration and a 64-fold difference in water consumption. This analysis, conducted at a national scale with a uniform methodology, confirms and extends field evidence from single-site studies [14–16], establishing humidity as the primary variable for pre-deployment screening.

The PV-to-load autonomy study produces an unexpected finding: The autonomy ratio is inversely correlated with the cooling capacity. Humid Black Sea sites have the greatest autonomy ratio (40.91) since near-zero misting activation leaves practically all PV production as surplus, whereas Hot-Dry Interior sites have the lowest autonomy (1.53) as prolonged misting operation produces significant pump-driven electrical demand. This outcome, which scales linearly with installed PV area, is a seasonal energy-balance indicator, not a promise of hour-by-hour off-grid operation. With 2-3 m^2 of PV area per module, the Hot-Dry Interior autonomy ratio reaches around 3.0-4.6, which offers a better operational margin for heavy misting applications.

Three broader design and deployment insights emerge from these results. First, adaptive control is essential: the rule-based misting logic prevents ineffective operation in humid conditions, aligns water and energy consumption with climatic suitability, and produces archetype-specific water-demand scaling (36-61 L per misting hour) that enables pre-deployment resource planning and integration with non-potable water sources at city scale. Second, MSPSCCs must be treated as climate-specific systems rather than universal outdoor cooling solutions; PV sizing, water supply strategy, and control threshold calibration must be adapted to local humidity and temperature conditions. Third, the MSPSCC functions as a complementary intervention that fills the response gap left by permanent UHI mitigation strategies, reflective surfaces, green roofs, and urban trees, which are capital-intensive and poorly responsive to acute heat events: in hot-dry and semi-arid contexts it delivers targeted active cooling; in persistently humid contexts it retains value as a passive solar shading and PV-powered amenity structure.

To the best of the authors' knowledge, this study is among the first studies to evaluate the climate-dependent joint performance of PV energy autonomy and evaporative spray cooling at national scale using a uniform methodology, and the first to apply climate archetype classification as a transferable pre-deployment screening framework for solar-powered misting systems. The sensitivity analysis in Section 4.7 confirms that the ordering of archetypes by misting feasibility is robust to moderate variations in control thresholds. Although the study does not resolve pedestrian-level airflow or thermal comfort fields, it establishes a reproducible basis for identifying suitable climatic contexts and guiding the next stage of detailed simulation, prototyping, and field validation.

 doi:10.20944/preprints202605.0695.v1

Future work should proceed in four directions. First, pilot deployments in representative Hot-Dry Interior and Semi-Arid Plateau locations combined with field measurements of mist-induced air temperature reduction and UTCI improvement are needed to validate and quantify the comfort outcomes implied by the feasibility results. Second, for typical urban forms within each archetype, site-specific CFD or microclimate modelling should help to address droplet evaporation, airflow interaction, and pedestrian-level cooling distributions. Third, resource efficiency in certain implementations will be enhanced by control threshold optimization linking T_{set} and RH_{max} to local UTCI-based comfort standards and occupancy profiles. Fourth, lifecycle cost analysis and techno-economic evaluation would round out the body of data required to back city-scale rollout choices.

As urban heat stress intensifies under climate change, scalable, resource-efficient, and rapidly deployable outdoor cooling solutions will be in increasing demand. The transferable, data-driven screening framework presented here supports climate-responsive deployment of PV-powered spray cooling infrastructure and contributes to the broader objective of designing public outdoor spaces that are more thermally resilient, energy-aware, and responsive to acute urban heat events.

Supplementary Materials: The following supporting information can be downloaded at the website of this paper posted on Preprints.org.

Data Availability Statement: The TMYx (2009-2023) climate data used in this study are publicly available from the OneBuilding repository (Climate.OneBuilding.org) [29]. The processed city-level and archetype-level performance datasets and the Python simulation notebook are available from the corresponding author upon reasonable request, as they contain proprietary intermediate calculation structures related to an ongoing broader research project. The full set of raw EPW files for all 110 locations is not hosted in a supplementary repository due to data volume constraints; readers are directed to download these directly from the OneBuilding repository using the station identifiers listed in Supplementary Table S1.

Appendix A. System Parameters and Operational Assumptions

Table A1 summarizes the baseline parameters used in the performance evaluation. Physical and scientific justification for each parameter is provided in Sections 2.2 and 2.3.

Table A1. Baseline parameters used in PV generation, electrical load, and water-use calculations.

Category	Parameter	Symbol	Value	Unit	Justification / cross-reference
Geometry	Canopy module footprint	–	4 × 4	m^2	Pedestrian-scale reference; catchment area in Eq. (5)
	Deployment configuration	–	Linear array	–	Reference case; per-module results apply to all configurations
PV system	Active PV area (normalized)	A_{pv}	1.0	m^2	Normalized basis; all results scale linearly with actual area
	Module efficiency (STC)	η_{pv}	0.20	–	Commercial monocrystalline Si; PVWatts default [28]
	Temperature coefficient	γ	−0.004	$°C^{-1}$	Negative for crystalline Si; PVWatts [28]; Eq. (1)
	Surface tilt	–	Latitude-based	°	Fixed, south-facing; maximizes annual yield
	Azimuth	–	180	°	South-facing; northern hemisphere
	Transposition model	–	Isotropic sky	–	Consistent with PVWatts [28]; Sect. 2.3.1

 doi:10.20944/preprints202605.0695.v1

	SAPM coeff. a	a	−3.56	–	Glass/polymer open-rack [28]; Sect. 2.3.1
	SAPM coeff. b	b	−0.075	–	Glass/polymer open-rack [28]; Sect. 2.3.1
Electrical loads	Pump power (ON)	P_{pump}	250	W	High-pressure misting pump; dominant load; Sect. 2.2.4
	Controls + sensors (ON)	P_{ctrl}	8	W	Microcontroller and sensors; Sect. 2.2.4
	Standby power (OFF)	P_{std}	2	W	Idle electronics; all inactive time steps; Sect. 2.2.4
Energy storage	Usable battery capacity	–	1.0	kWh	Feasibility indicator; not a multi-day SoC simulation; Sect. 2.3.1
Misting system	Nozzle flow rate (full duty)	$\dot{m}_u$	2.0	L min^{-1}	Per module; enters Eq. (4)
	Droplet size range	–	Micron-tens of microns	–	Complete evaporation; minimal wetting [14,18]
Adaptive control	Activation temperature	T_{set}	32	°C	UTCI moderate heat-stress boundary [27]; consistent with [14,18]
	Humidity deactivation	RH_{max}	65	%	Evaporation suppressed; wetting risk above this value [16]; Sect. 2.3.2
	Min. POA irradiance	G_{min}	200	W m^{-2}	Restricts to sunny periods; Sect. 2.3.2
	Duty-cycle ramp	ΔT	8	°C	Duty 0.25 at T_{set} → 1.0 at $T_{set}+\Delta T$ (low RH); Sect. 2.3.2
Simulation scope	Analysis period	–	June-August	–	Peak summer heat stress and PV generation
	Daytime window	–	10:00-18:00	local solar time	Peak occupancy and irradiance; Sect. 2.4.1
	Time step	–	1	h	EPW hourly resolution
	Climate dataset	–	TMYx 2009-2023	–	OneBuilding [29]; 110 EPW files

STC = standard test conditions. SoC = state of charge. POA = plane of array. SAPM = Sandia Array Performance Model. PV energy and autonomy values are per 1 m² PV area and scale linearly with installed area. Battery capacity is a feasibility indicator only, not a detailed multi-day SoC simulation.

Appendix B. Summer Climate Archetype Definitions

The 110 analyzed locations were classified into six summer climate archetypes using k-means clustering (k = 6) of five standardized summer daytime variables, as described in Section 2.4.2. Table B1 defines each archetype by its dominant climatic characteristics and summarizes its implications for spray cooling system behavior, with performance values updated to match the corrected results of Table 3. The full location-level dataset is provided as Supplementary Table S1.

Table B1. Definitions and spray cooling implications of the six identified summer climate archetypes.

Climate archetype	N sites	Dominant summer characteristics	Spray cooling system behavior

 doi:10.20944/preprints202605.0695.v1

Hot–Dry Interior	20	Highest mean T_a (~33.5 °C); lowest mean RH (~24%); high GHI	Longest misting (~503 h); highest water (~30 486 L/module); lowest autonomy (~1.53); primary high-benefit deployment context; PV area of 2–3 m² recommended
Semi-Arid Plateau	27	Moderate-to-high T_a (~27 °C); low-to-moderate RH (~31%); strong irradiance	Moderate misting (~99 h); balanced water (~4 312 L); autonomy ~13; baseline 1 m² PV sufficient; most widespread archetype
Humid Mediterranean Coastal	17	High T_a (~30 °C); moderate RH (~47%); high GHI	Meaningful misting (~234 h); water ~9 573 L; autonomy ~12; passive shading plus intermittent active cooling
Temperate Coastal	17	Moderate T_a (~29 °C) and RH (~51%); moderate irradiance	Intermittent misting (~145 h); water ~5 710 L; autonomy ~7; wider inter-site variability within archetype
Cold Continental Highland	10	Moderate T_a (~28 °C); moderate RH (~55%); high GHI despite altitude	Limited misting (~97 h); water ~3 466 L; high autonomy (~25); system functions primarily as shading structure with PV surplus
Humid Black Sea	19	Lowest T_a (~25 °C); highest RH (~62%); lowest GHI	Minimal misting (~13 h); negligible water (~478 L); highest autonomy (~41) reflects near-zero load; system operates as passive solar canopy only

N = number of EPW locations per archetype. Performance values are archetype means from Table 3. Archetype labels describe dominant summer characteristics and should not be interpreted as formal climatological zones.

References

1. Johri, S., Selvakumar, P., Satyanarayana, P., Das, A., Gupta, S., & Bhattacharya, S. (2025). Urbanization and Energy: The Nexus of Global Challenges. In F. Özsungur, M. Chaychi Semsari, & H. Küçük Bayraktar (Eds.), *Geopolitical Landscapes of Renewable Energy and Urban Growth* (pp. 453-478). IGI Global Scientific Publishing. https://doi.org/10.4018/979-8-3693-8814-3.ch016
2. Jabbar, H.K., Hamoodi, N., & Al-Hameedawi, A.N. (2022). Urban heat islands: a review of contributing factors, effects and data. *IOP Conference Series: Earth and Environmental Science*, 1129, 012038. https://doi.org/10.1088/1755-1315/1129/1/012038
3. de Souza, C.H. (2024). Quantitative Analysis of the Impact of Urban Heat Island Intensity on Air Conditioning Energy Consumption in São Paulo. *J. of Progress in Eng. and Physical Sci.*, 3(4), 53-55. Retrieved from https://www.pioneerpublisher.com/jpeps/article/view/1125.
4. Santamouris, M., Papanikolaou, N., Livada, I., Koronakis, I., Georgakis, C., Argiriou, A., Assimakopoulos, D.N. (2001). On the impact of urban climate on the energy consumption of buildings, *Solar Energy*, 70:3, 201-216, doi.org/10.1016/S0038-092X (00)00095-5.
5. Zhang, M., Chen, S., Ren, Y., Yu, Z., & Yu, J. (2025). Hourly cooling demand prediction through a bottom-up model in London. *International Journal of Green Energy*, 22(11), 2197–2210. https://doi.org/10.1080/15435075.2025.2452220.
6. Takane, Y., Kikegawa, Y., Hara, M. et al. (2019). Urban warming and future air-conditioning use in an Asian megacity: importance of positive feedback. *npj Clim Atmos Sci.*, 2, 39. https://doi.org/10.1038/s41612-019-0096-2.
7. Schlosberg, D. (2012). Climate Justice and Capabilities: A Framework for Adaptation Policy. *Ethics & International Affairs*, 26(4), 445–461. https://doi.org/10.1017/S0892679412000615
8. Jandaghian, Z., & Colombo, A. (2024). The Role of Water Bodies in Climate Regulation: Insights from Recent Studies on Urban Heat Island Mitigation. *Buildings*, 14(9), 2945. https://doi.org/10.3390/buildings14092945.

 doi:10.20944/preprints202605.0695.v1

9. Ziaeemehr, B., Jandaghian, Z., Ge, H., Lacasse, N., & Moore, T. (2023). Increasing Solar Reflectivity of Building Envelope Materials to Mitigate Urban Heat Islands: A State-of-the-Art Review. *Buildings*, 13:11, 2868. doi.org/10.3390/buildings13112868
10. Qi, J., He, B.J. (2023). Urban Heat Mitigation Strategies. In: Cheshmehzangi, A., He, BJ., Sharifi, A., Matzarakis, A. (eds) *Climate Change and Cooling Cities*. Urban Sustainability. Springer, Singapore. https://doi.org/10.1007/978-981-99-3675-5_2.
11. Yang, J., Kumar, D.I.M., Pyrgou, A., Chong, A., Santamouris, M., Kolokotsa, D., Lee, S.E. (2018). Green and cool roofs' urban heat island mitigation potential in tropical climate, *Solar Energy*, 173, 597-609, doi.org/10.1016/j.solener.2018.08.006.
12. Irfeey, A.M.M., Chau, H.-W., Sumaiya, M.M.F., Wai, C.Y., Muttil, N., & Jamei, E. (2023). Sustainable Mitigation Strategies for Urban Heat Island Effects in Urban Areas. *Sustainability*, *15*(14), 10767. https://doi.org/10.3390/su151410767
13. Almusaed, A. (2011). *Cooling by Indirect Evaporative Systems*. In: Biophilic and Bioclimatic Architecture. Springer, London. https://doi.org/10.1007/978-1-84996-534-7_31.
14. Ulpiani, G., Di Giuseppe, E., Di Perna, C., et al. (2019). Thermal comfort improvement in urban spaces with water spray systems: field measurements and survey. Building and Environment, 156, 46–61. https://doi.org/10.1016/j.buildenv.2019.03.042
15. Tian, J., & Li, N. (2024). Mist Spraying as an Outdoor Cooling Spot in Hot-Humid Areas: Effect of Ambient Environment and Impact on Short-Term Thermal Perception. Buildings, 14(2), 336. https://doi.org/10.3390/buildings14020336
16. Gao, Y., et al. (2025). Evaporative cooling mist-spray system to enhance thermal comfort in urban outdoor premises. Energy and Buildings. https://doi.org/10.1016/j.enbuild.2025.015646
17. Stojanovic, Dj., Vujovic, M., Ding, Y., & Katic, M. (2023). Context-Aware Module for Evaporative Cooling in the Outdoor Built Environment. International Journal of Architectural Computing, 21(1), 100–119. https://doi.org/10.1177/14780771221095307
18. Ulpiani, G., & Zinzi, M. (2023). Experimental assessment of the heat mitigation potential of an urban cooling shelter: Combining water misting with solar shading, wind shield, and smart control. *Energy and Buildings*, 299, 113623. https://doi.org/10.1016/j.enbuild.2023.113623
19. Eduard, R., Ruslan, W., Iskandar, I., & Setyanto, D. (2022). Setting Temperature and Humidity with a Misting System in a Pilot Greenhouse at Cisauk-Tangerang, Indonesia. *Applied Sciences*, 12(18), 9192. https://doi.org/10.3390/app12189192
20. Malbog, M. A. F., Castro, J. C., Cunanan, C. F., Pateña, N. M., & Bastes, B. M. (2020). MISTMATIC: Automatic Misting Control System for Indoor Garden with Rule-Based Approach. *J. of Adv. Trends in Computer Sci. and Eng*., 9(4), 6471–6476. https://doi.org/10.30534/ijatcse/2020/332942020
21. Formolli, M., Croce, S., Vettorato, D., Paparella, R., Scognamiglio, A., Mainini, A.G., & Lobaccaro, G. (2022). Solar Energy in Urban Planning: Lesson Learned and Recommendations from Six Italian Case Studies, *Applied Sciences*, 12:6, 2950. doi.org/10.3390/app12062950
22. Santos, T., Lobato, K., Rocha, J., & Tenedório, J. A. (2020). Modeling Photovoltaic Potential for Bus Shelters on a City-Scale: A Case Study in Lisbon. *Applied Sciences*, 10(14), 4801. https://doi.org/10.3390/app10144801
23. Alikhanova, A., Kakimzhan, A., Mukhanov, A., & Rojas-Solórzano, L. (2019). Design of a bus shelter based on green energy technologies for extreme weather conditions in Nur-Sultan, Kazakhstan. *Sustainable Energy Technologies and Assessments*, 36, 100544. https://doi.org/10.1016/j.seta.2019.100544
24. Sánchez-Aparicio, M., González-González, E., Martín-Jiménez, J. A., & Lagüela, S. (2023). Solar Potential Analysis of Bus Shelters in Urban Environments: A Study Case in Ávila (Spain). *Remote Sensing*, 15(21), 5189. https://doi.org/10.3390/rs15215189
25. Abdulmouti, H., Skaf, Z., Alnajjar, F., Ali, L., Mehiar, D., & Abousamra, R. (2025). Towards Renewable Urban Landscapes: Exploring Photovoltaic Panel Integration-A Case Study. *International Journal of Energy for a Clean Environment*, 26(2), 77–93. https://doi.org/10.1615/InterJEnerCleanEnv.2024049846
26. Ouyang, W., Ren, G., Tan, Z., Li, Y., Ren, C. (2024). Natural shading vs. artificial shading: A comparative analysis of their cooling efficacy in extreme hot weather, *Urban Climate*, 55, 101870. https://doi.org/10.1016/j.uclim.2024.101870.

 doi:10.20944/preprints202605.0695.v1

27. Błażejczyk, K., Jendritzky, G., Bröde, P., Fiala, D., Havenith, G., Epstein, Y., Psikuta, A., & Kampmann, B. (2013). Introduction to the universal thermal climate index (UTCI). *Geographia Polonica*, 86(1), 5–10. https://doi.org/10.7163/GPol.2013.1
28. Dobos, A.P. (2014). PVWatts Version 5 Manual (NREL/TP-6A20-62641). *National Renewable Energy Laboratory* (NREL). https://www.nrel.gov/docs/fy14osti/62641.pdf.
29. Lawrie, L.K., Crawley, D.B., (2022). Development of Global Typical Meteorological Years (TMYx). *Building performance simulation climate data*. Available at: https://climate.onebuilding.org